J. Astrophys. Astr. (2004) **25,** 129–141

On the Origin of the Wide HI Absorption Line towards Sgr A*

K. S. Dwarakanath[1], W. M. Goss[2], J. H. Zhao[3] & C. C. Lang[4]
[1]*Raman Research Institute, Sadashivanagar, Bangalore 560 080, India.*
e-mail: dwaraka@rri.res.in
[2]*National Radio Astronomy Observatory, PO BOX O, Socorro, NM 87801.*
e-mail: mgoss@aoc.nrao.edu
[3]*Harvard-Smithsonian Center for Astrophysics, Cambridge, MA 02138.*
e-mail: jzhao@cfa.harvard.edu
[4]*Department of Physics and Astronomy, University of Iowa, Iowa City, IA 52242.*
e-mail: cornelia-lang@uiowa.edu

Received 2004 May 7; accepted 2004 October 19

Abstract. We have imaged a region of $\sim 5'$ extent surrounding Sgr A* in the HI 21 cm-line absorption using the Very Large Array. A Gaussian decomposition of the optical depth spectra at positions within $\sim 2'$ (~ 5 pc at 8.5 kpc) of Sgr A* detects a wide line underlying the many narrow absorption lines. The wide line has a mean peak optical depth of 0.32 ± 0.12 centered at a mean velocity of $V_{\rm lsr} = -4 \pm 15$ km s^{-1}. The mean full width at half maximum is 119 ± 42 km s^{-1}. Such a wide line is absent in the spectra at positions beyond $\sim 2'$ from Sgr A*. The position-velocity diagrams in optical depth reveal that the wide line originates in various components of the circumnuclear disk (radius $\sim 1.3'$) surrounding Sgr A*. These components contribute to the optical depth of the wide line in different velocity ranges. The position-velocity diagrams do not reveal any diffuse feature which could be attributed to a large number of HI clouds along the line of sight to Sgr A*. Consequently, the wide line has no implications either to a global population of shocked HI clouds in the Galaxy or to the energetics of the interstellar medium as was earlier thought.

Key words. Galaxy: nucleus—radio lines: ISM.

1. Introduction

The Galaxy harbours a compact radio source Sgr A* at its center. The intrinsic size of Sgr A* is constrained by the most recent multi frequency VLBA observations to be 24 ± 2 Schwarzschild radius (~ 2 AU for a 4×10^6 M$_\odot$ black hole) at 43 GHz and scales as $\lambda^{1.6}$ (Bower *et al*. 2004). A filamentary region of ionised gas, Sgr A West of ~ 2.5 pc in extent ($\sim 1'$) surrounds Sgr A* (Lo & Claussen 1983; Roberts & Goss 1993). Both Sgr A* and Sgr A West are surrounded by a ring of molecular material called the circumnuclear disk (CND) the outer edge of which has been traced up to ~ 7 pc (Gusten *et al*. 1987). Surrounding (in projection) both Sgr A* and Sgr A West is the supernova remnant Sgr A East with a radius of ~ 5 pc (Ekers *et al*. 1983,

Maeda *et al*. 2002). The supernova remnant is in close proximity to Sgr A West and is expanding into a molecular cloud complex (Pedlar *et al*. 1989).

The compact source Sgr A* and its surroundings have been a target of HI 21 cm-line measurements for many years. A number of absorption and emission features with a radial velocity range of $-190\,\mathrm{km\,s^{-1}}$ to $+135\,\mathrm{km\,s^{-1}}$ have been detected towards this region which shows little Galactic rotation (Liszt *et al*. 1983). However, many of the components show evidence of non-circular motion. Some of the anomalous absorption features are the $-53\,\mathrm{km\,s^{-1}}$ feature due to the 'Expanding 3-kpc Arm', the $-135\,\mathrm{km\,s^{-1}}$ feature due to the 'Expanding Molecular Ring', and the $+50\,\mathrm{km\,s^{-1}}$ feature due to the molecular cloud into which Sgr A East is expanding.

Early HI 21 cm-line observations towards Sgr A* were carried out using the Parkes Interferometer with a resolution of $3'$ (Radhakrishnan *et al*. 1972). An analysis of the HI 21 cm-line absorption spectrum towards Sgr A* revealed, apart from many familiar features, an unexpected wide, shallow component (Radhakrishnan & Sarma 1980, RS1). This component was centered at $V_{\mathrm{lsr}} = -0.22\,\mathrm{km\,s^{-1}}$ with a peak optical depth of 0.3 and a velocity dispersion of $35\,\mathrm{km\,s^{-1}}$ (full width at half maximum (FWHM) $\sim 80\,\mathrm{km\,s^{-1}}$). This component was attributed to a new population of shocked HI clouds in the Galaxy observed along the line of sight towards Sgr A* (Radhakrishnan & Srinivasan 1980, RS2). Estimates indicated that the kinetic energy in these clouds was ~ 100 times that in the standard HI clouds with consequent implications to the energetics of the interstellar medium.

Subsequent HI absorption measurements towards Sgr A* using the Westerbork Synthesis Radio Telescope (WSRT) did not confirm the existence of this wide line and placed an upper limit to its peak optical depth of 0.1 (Schwarz, Ekers & Goss 1982). Around the same time, Shaver *et al*. (1982), and Anantharamaiah *et al*. (1984) made an analysis of the differences between the terminal velocities of HI absorption spectra and the recombination line velocities in the directions of 38 HII regions of known distances. This analysis provided estimates of the number densities and random velocity dispersions of interstellar HI clouds. Their results supported the earlier postulate of shocked HI clouds in the Galaxy. However, Kulkarni & Fich (1985) found that these results were easily confused by many known systematic effects. After accounting for all these effects they found that the results of Shaver *et al*. (1982) and Anantharamaiah *et al*. (1984) were quite uncertain. Using HI emission data throughout the Galactic Plane, Kulkarni & Fich (1985) suggested that the amount of HI in the high velocity dispersion HI concentrations is an order of magnitude less than proposed by RS2.

More recently, HI absorption measurements towards Sgr A* were carried out using the Australia Telescope Compact Array (ATCA) (Rekhesh Mohan 2003, RM). These observations confirmed the existence of a wide (FWHM $\sim 120\,\mathrm{km\,s^{-1}}$) and shallow ($\tau_{\mathrm{peak}} \sim 0.3$) absorption feature towards Sgr A*. The discrepancy between the earlier two observations can be attributed to the smaller velocity coverage used in the WSRT observations. The spatial distribution of this spectral feature could not be obtained from the recent ATCA observations due to limited visibility coverage and poor sensitivity. A recent HI absorption measurement towards the Galactic Anticenter using the WSRT detected no such wide line to a 3σ optical depth limit of 0.006 indicating that the wide HI absorption line detected towards Sgr A* is not ubiquitous (RM). Thus, the nature of the wide HI absorption line towards Sgr A* remained unclear.

From the earlier HI absorption measurements towards Sgr A*, it is clear that a large velocity coverage $\sim 600\,\mathrm{km\,s^{-1}}$ is required to detect the wide HI absorption line. A

velocity resolution $\sim 1\,\mathrm{km\,s^{-1}}$ is also necessary to identify and remove the narrow (FWHM $\sim$ a few km $\mathrm{s^{-1}}$) HI absorption lines which are detected along most lines of sight in the Galaxy and more so towards Sgr A*. In addition, an excellent visibility coverage is necessary to image the complex continuum and HI distribution observed towards Sgr A* and its immediate surroundings. Therefore, we have undertaken a high spectral and spatial resolution HI absorption study of the Sgr A* and its immediate surroundings ($\sim 5'$) with the Very Large Array in order to determine the spatial distribution of the shallow and wide HI absorption component, to characterize its physical properties, and to determine its origin and physical relationship to the center of the Galaxy. In section 2, we present the observations; in section 3, the data analysis; and in section 4, the discussion.

2. Observations and imaging

The observations were carried out using the Very Large Array (VLA) in the 36 km (A), 11 km (B), 3 km (C), and 1 km (D) configurations during January – October 2002. The total integration times in each of these configurations were $\sim$13, 9, 2 and 2 hours respectively. The field center of these observations was α (2000) $= 17^{\mathrm{h}}\,45^{\mathrm{m}}\,40^{\mathrm{s}}.049$, and δ (2000) $= -29^{\circ}\,00'\,27''.98$. The standard observing modes of the VLA spectrometer cannot provide both the required velocity coverage ($\sim 600\,\mathrm{km\,s^{-1}}$) and velocity resolution ($\sim 1\,\mathrm{km\,s^{-1}}$). Therefore, two overlapping bands each with 1.56 MHz bandwidth and 255 spectral channels were arranged to cover the desired velocity range ($\pm 300\,\mathrm{km\,s^{-1}}$) for the Galactic HI 21 cm-line. There were 25 overlapping channels in the flat portions of the bands. After precise bandpass calibration the two bands were combined together to produce a final data base with a velocity coverage of 590 km $\mathrm{s^{-1}}$ at a spectral resolution of 1.3 km $\mathrm{s^{-1}}$ after Hanning smoothing.

2.1 *Imaging*

The calibration and imaging were carried out using the Astronomical Image Processing System (AIPS). Using the data from the A + B + C + D arrays CLEANed image cubes containing both the continuum and the spectral line data were produced. Continuum images were produced from the respective image cubes by averaging the line-free channels. Spectral line image cubes were produced by constructing a linear fit to the continuum in the line-free channels as a function of the channels and subtracting this linear fit from all channels. Optical depth image cubes were produced by suitably combining the spectral line image cubes and the respective continuum images. A continuum image of the region surrounding Sgr A* is shown in Fig. 1. Representative optical depth spectra at the four positions indicated in this figure are shown in Fig. 2.

Using the data from the C + D arrays, three sets of CLEANed image cubes containing both the continuum and the spectral line data were produced. These three data sets included all visibilities, the visibilities beyond the inner 40 m, and the visibilities beyond the inner 100 m respectively. The upper limit to the included range of visibilities in all the three images was $\sim$3400 m. Continuum images and optical depth image cubes were produced following the procedure described earlier. The contamination due to HI emission was minimal in all the images. However, of the three sets of images, the second set of images had the best spatial resolution and the maximum spatial extent

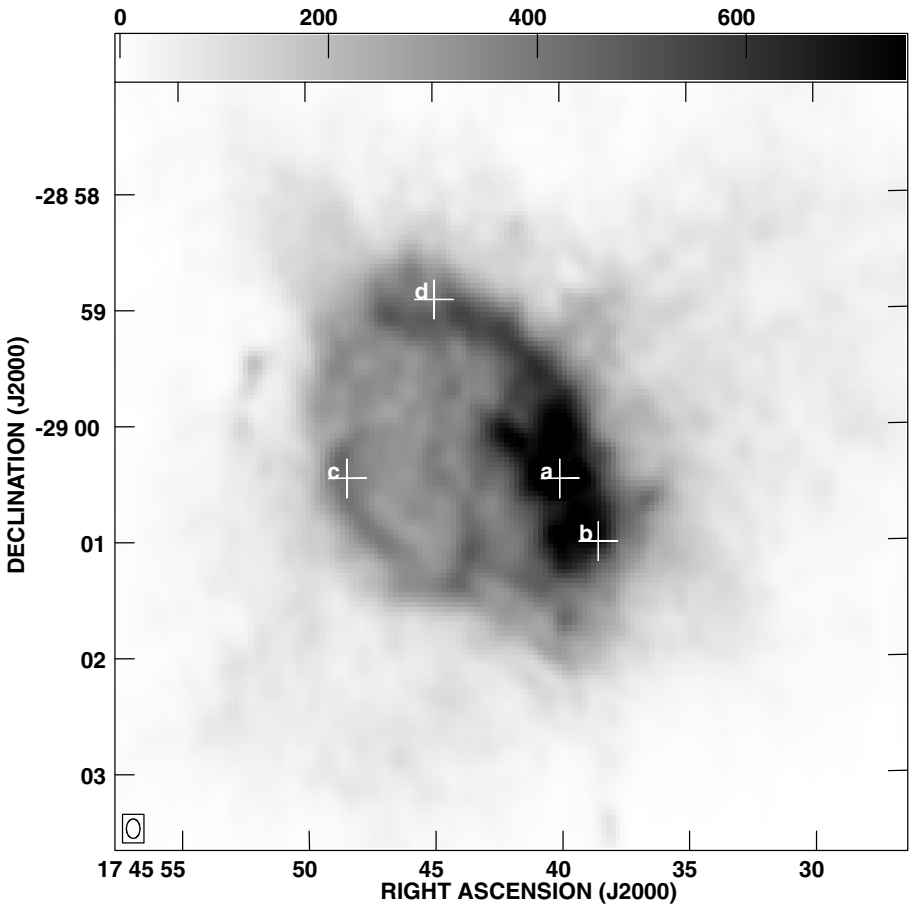

Figure 1. A radio continuum image made from the A+B+C+D array data. The synthesised beam, $10'' \times 7''$ at a position angle of 0°, is shown at the bottom left hand corner. The RMS is 9 mJy/beam. The grey scale flux density range is 0 to 750 mJy/beam. The four crosses marked a, b, c, and d indicate the positions at which the four spectra shown in Fig. 2 were obtained respectively. The cross marked 'a' is the position of Sgr A*.

of the optical depth distribution. Since one of the primary motivations of the current observations was to estimate the spatial distribution of the wide HI absorption line, the second set of images was used in further analysis. A continuum image of the region surrounding Sgr A* from the second data set is shown in Fig. 3. This image has a synthesized beam of $40'' \times 20''$ (position angle $= 0^\circ$) with an RMS of 30 mJy beam^{-1}.

The data from the A+B+C+D arrays provides higher spatial resolution compared to the data from the C+D arrays. However, the radio continuum extent imaged from the high resolution data is rather limited (Fig. 1). The more extended continuum features detected in the C + D arrays data (Fig. 3) are resolved in the high resolution data. The limited extent of the radio continuum precludes the high resolution images being used for tracing the spatial extent of the wide absorption line. However, the high resolution data are used as an independent check of the results from the low resolution data where both are available.

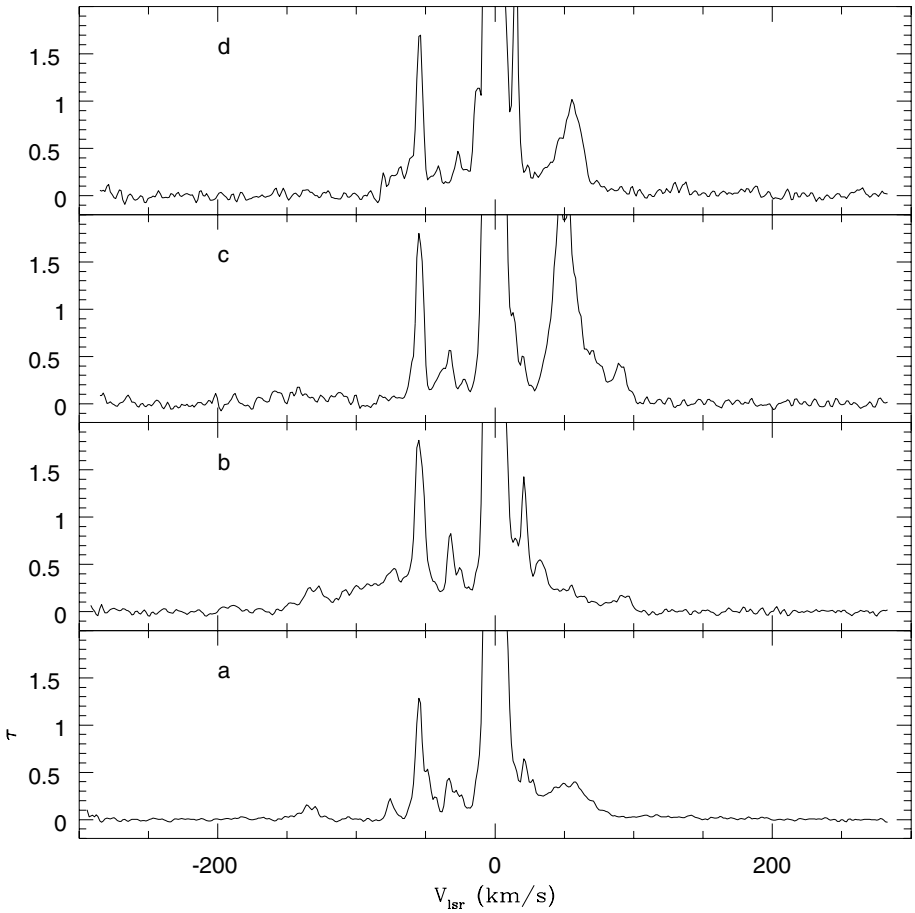

Figure 2. Optical depth spectra from the A + B + C + D array data. The four spectra correspond to the four positions marked in Fig. 1 respectively. Gaussian analysis of the spectra detects a wide line (FWHM ~ 120 km s^{-1}) apart from the many narrow lines that are evident. In many spectra, like for example, the one marked 'b', such a wide line is evident as a broad shoulder underneath the narrow lines.

3. Analysis of the optical depth spectra and images

The motivation for the current observations are (a) to confirm the existence of a wide velocity component in the HI absorption spectra towards Sgr A* and (b) to understand its possible origin. The HI absorption spectra in the Galactic plane are dominated by the presence of deep (optical depth ~ 0.5) and relatively small dispersion ($\sim$ a few km s^{-1}) lines. The presence of a large velocity dispersion ($\sim$30–50 km s^{-1}) HI absorption component can manifest as a broad shoulder underlying the narrow lines in an optical depth spectrum. Often a visual inspection can reveal this shoulder. Representative optical depth spectra from the C + D array data at the positions marked in Fig. 3 are displayed in Figs. 4 and 5. The spectra in Fig. 4 at positions within $\sim 2'$ from Sgr A* reveal such a shoulder which is absent in the spectra at positions outside $\sim 2'$ from Sgr A* (Fig. 5). However, a quantitative analysis of the optical depth spectra is necessary to confirm these visual impressions.

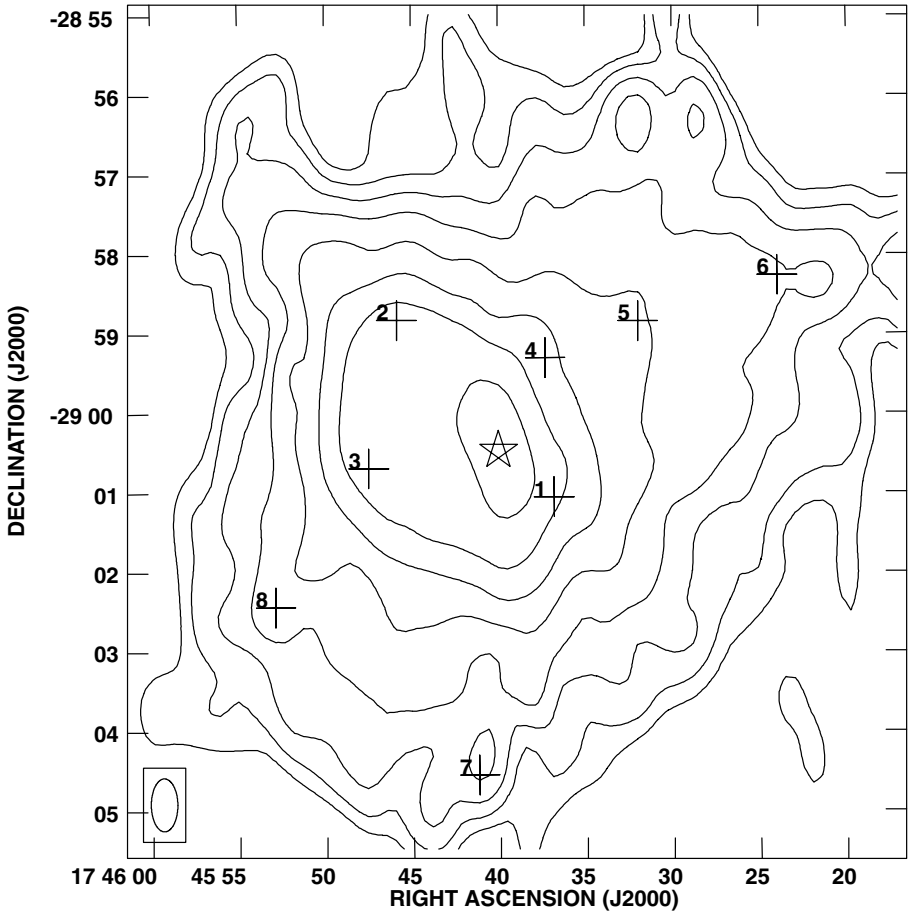

Figure 3. A radio continuum image made from the C + D array data. The synthesised beam, $40'' \times 20''$ at a position angle of 0°, is shown at the bottom left hand corner. The RMS is 30 mJy/beam. Contours start at 50 mJy/beam and increase successively by a factor of 2. The star marks the position of Sgr A*. The crosses mark the positions at which the optical depth spectra shown in Figs. 4 and 5 were extracted.

The HI 21 cm-line absorption or emission studies carried out in the past indicate that most of these profiles are well fit by Gaussians. The Gaussian decomposition of the optical depth spectrum was carried out by a code written for this purpose based on the Levenberg–Marquardt Method (Numerical Recipes in Fortran 1992). This method minimizes the χ^2 by computing both its first and second derivatives with respect to the variables (parameters of the Gaussians to be fitted) and approaching a minimum. The desired number of input Gaussians are fit to the data simultaneously and the best-fit model is derived after a suitable number of iterations during which the parameters of the input Gaussians are varied to obtain the minimum χ^2. Two examples illustrating such an analysis are given in Figs. 6 and 7. The data in Figs. 6 and 7 are the spectra marked '1' and '5' in Figs. 4 and 5 respectively. The best-fit model for the data in Fig. 6 is displayed in the second panel from the top in Fig. 6. The third panel from top is the residual spectrum (data-model), consistent with noise. The bottom panel in

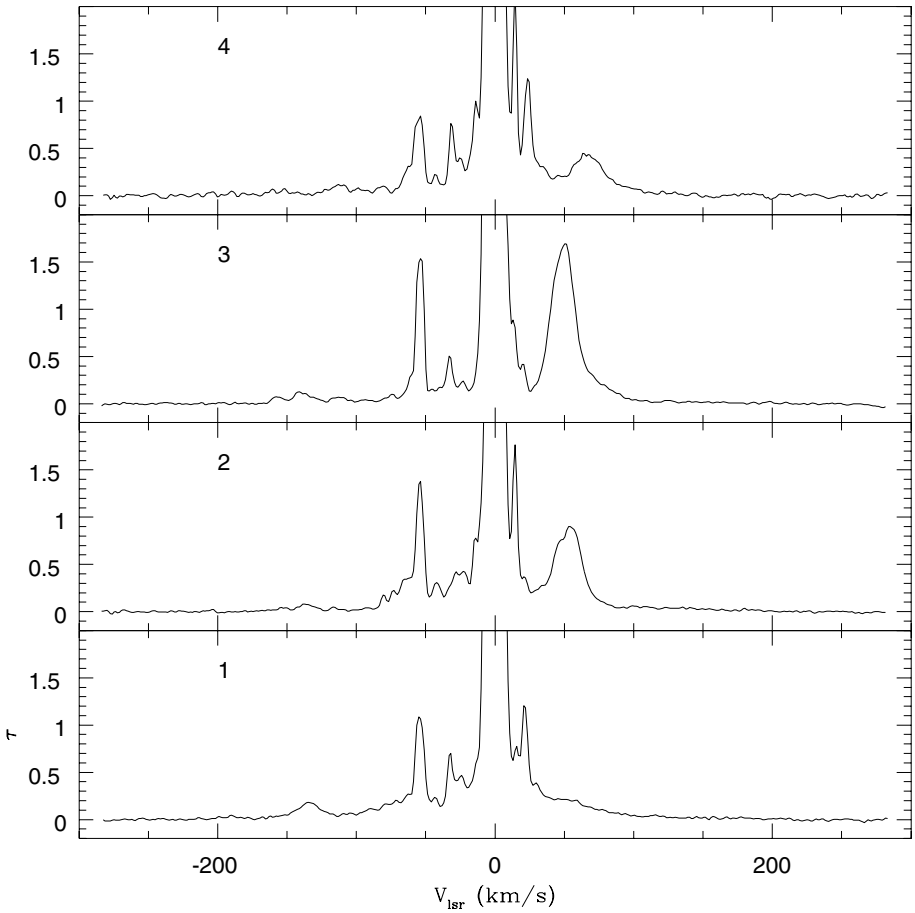

Figure 4. Optical depth spectra from the C+D array data at the positions 1, 2, 3 and 4 respectively marked in Fig. 3. These spectra are representative of the spectra at positions within $\sim 2'$ from Sgr A*. A Gaussian analysis detects a wide line with mean values of $V_{\rm lsr} = -4 \pm 15\,{\rm km\,s^{-1}}$, $\delta V_{1/2} = 119 \pm 42\,{\rm km\,s^{-1}}$, and $\tau_{\rm peak} = 0.32 \pm 0.12$ in the spectra at positions within $\sim 2'$ from Sgr A*.

Fig. 6 displays the residual when the 11 narrow lines in the model are subtracted from the data. A wide line of FWHM $\sim 129\,{\rm km\,s^{-1}}$ is detected in the data. The 11 narrow components have a mean FWHM of $12 \pm 8\,{\rm km\,s^{-1}}$, with the FWHMs in the range 4–24 km s^{-1}. The best-fit Gaussian model for the data in Fig. 7 has 8 components with a mean FWHM of $7 \pm 3\,{\rm km\,s^{-1}}$. No wide line is detected in this spectrum. The quantitative analysis confirms the visual impressions of these spectra.

A Gaussian decomposition of the optical depth spectra from the C + D array data at independent positions across the extent of the source (Fig. 3) was carried out. Such an analysis detected a wide line (FWHM $\sim 120\,{\rm km\,s^{-1}}$) in the spectra at positions within $\sim 2'$ of Sgr A*. No wide line was detected in the spectra at positions beyond $\sim 2'$ of Sgr A*. Wide lines of similar characteristics were also detected in the spectra from the high resolution images (Fig. 2).

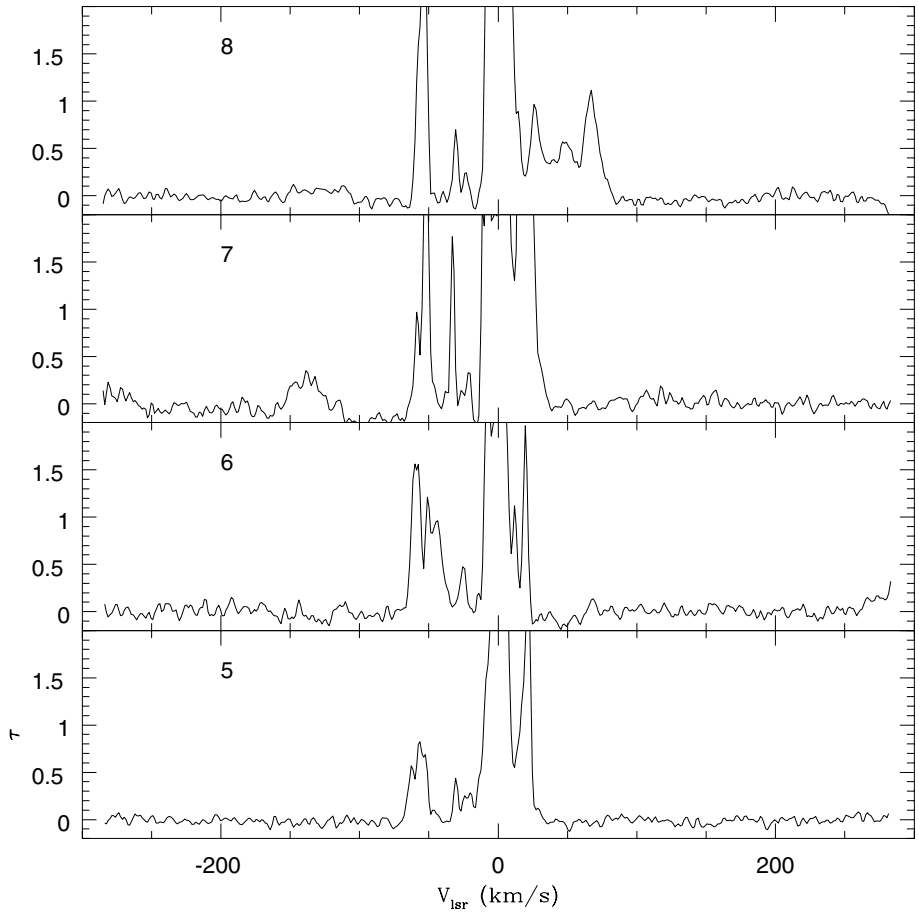

Figure 5. Same as in Fig. 4 but for positions 5, 6, 7 and 8 respectively. These spectra are representative of the spectra at positions beyond $\sim 2'$ from Sgr A*. A wide line of the kind detected in the spectra in Fig. 4 is absent in these spectra.

3.1 *Physical features associated with the wide line*

The position-velocity diagrams are an effective means to identify the physical features associated with spectral lines. As an illustrative example, two declination-velocity images are shown in Figs. 8 and 9, corresponding to the positions marked '1' and '5' respectively (Fig. 3). Both the figures are dominated by optical depth features which are parallel to declination and centered around $V_{\rm lsr} \sim 0,\ -25$ and $-50\,{\rm km\ s^{-1}}$. However, Fig. 8 shows high optical depth features at positive velocities ($\sim 100\,{\rm km\ s^{-1}}$) to the north of Sgr A*, and at negative velocities ($\sim -100\,{\rm km\ s^{-1}}$) to the south of Sgr A*. These two features form two ends of an inverted S-shaped feature (Fig. 8). Detailed modeling has shown that these features result due to the circumnuclear disk (CND) of mean radius 3.2 pc ($\sim 1.3'$) rotating about Sgr A* with a velocity $\sim 100\,{\rm km\ s^{-1}}$ (Liszt *et al*. 1985). Such an inverted S-shaped feature is absent in Fig. 9 due to the finite size of the CND. The optical depth spectrum at the position marked '1' (Figs. 3 and 4) is the spectrum at $\delta = -29^\circ\ 01'\ 03''$ in Fig. 8 and originates from the CND. The

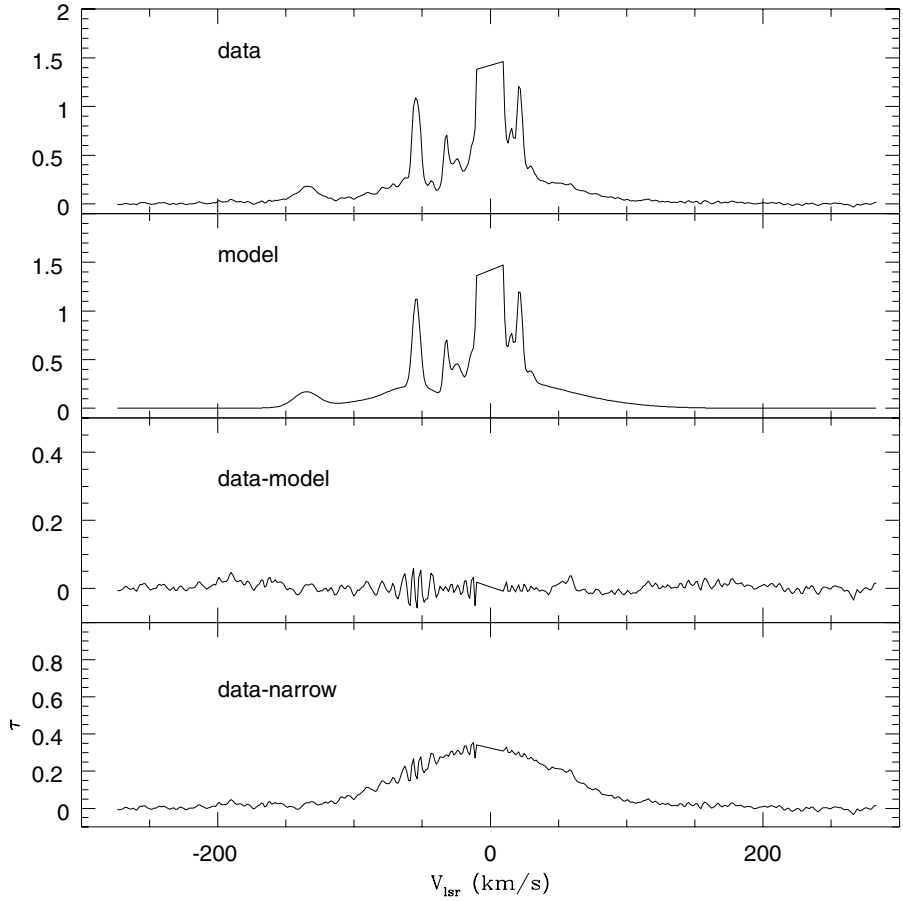

Figure 6. Gaussian decomposition. The data is the optical depth spectrum from the C + D array data (marked '1' in Figs. 3 and 4). The best-fit model consists of 11 narrow Gaussians with a mean FWHM of $12 \pm 8\,\mathrm{km\ s^{-1}}$ and a wide Gaussian of FWHM $129 \pm 1\,\mathrm{km\ s^{-1}}$. The residual (data-model) is consistent with noise. The bottom panel displays the residual when only the narrow lines in the model are subtracted from the data. This wide line is also evident in the data as a broad shoulder.

spectrum at the position marked '5' (Figs. 3 and 5) is the spectrum at $\delta = -28^\circ\ 58'\ 50''$ in Fig. 9.

Although the position-velocity plots demonstrate that the CND is responsible for the wide line, a more direct connection of the wide line to the CND is desirable. A comparison of the spatial distribution of the wide line parameters (central velocity, width, and peak optical depth) with the CND can bring out such a connection. The spatial distributions of the wide line parameters indicate some systematic behaviour in relation to the CND. However, the evidence is rather inconclusive. The basic limitation appears to be that the spatial resolution provided by the C+D arrays is coarse compared to the linear scales over which velocity gradients and turbulence exist in the region surrounding Sgr A* (Gusten *et al*. 1987). The data from the A + B + C + D arrays have adequate spatial resolution for this purpose, but has inadequate surface brightness to trace the spatial distribution of the wide line parameters.

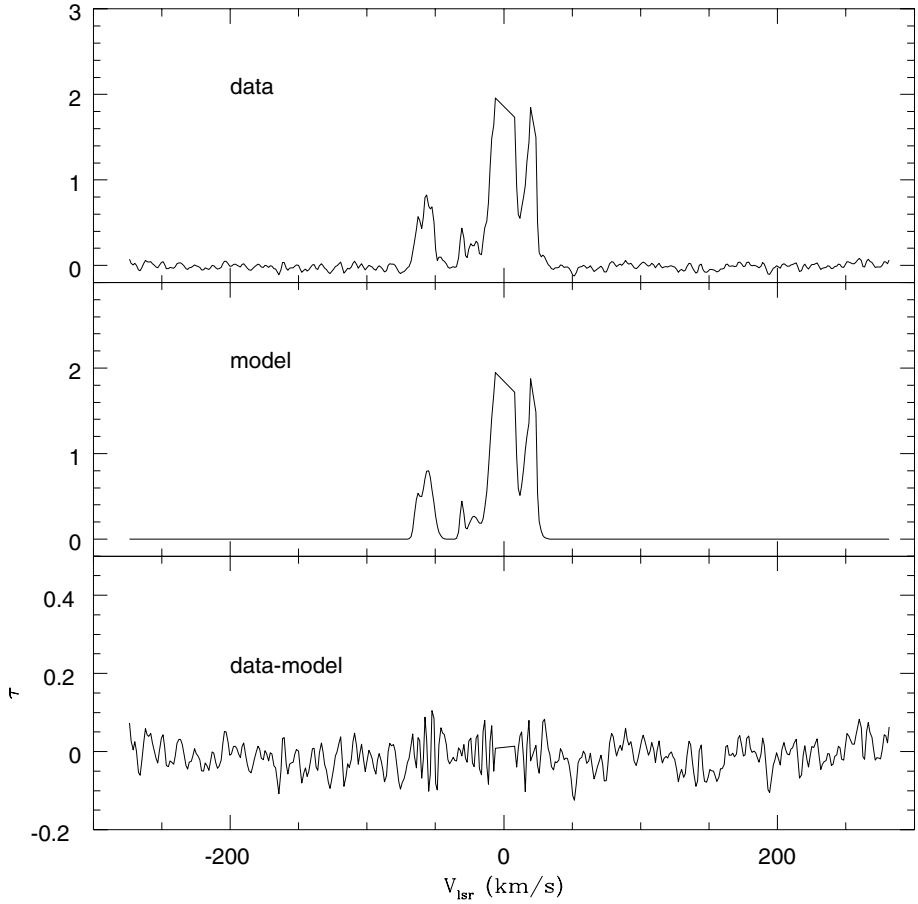

Figure 7. Gaussian decomposition. The data is the optical depth spectrum from the C + D array data (marked '5' in Figs. 3 and 5). The best-fit model consists of 8 narrow Gaussians with a mean FWHM of $7 \pm 3\,\mathrm{km\,s^{-1}}$. The residual (data-model) is consistent with noise. No wide line is detected in this spectrum.

4. Discussion

The current observations have demonstrated the existence of a wide line ($\delta V_{1/2} \sim 120\,\mathrm{km\,s^{-1}}$) in the optical depth spectra towards Sgr A* and its surroundings, confirming the early results of RS1. Since such a wide line is detected in the present observations towards positions within $\sim 2'$ from Sgr A*, it is understandable that the Parkes Interferometer observations towards Sgr A* detected such a wide line even with a poorer resolution of $\sim 3'$. No wide line was detected in the current observations at positions beyond $\sim 2'$ from Sgr A*.

A comparison of the optical depth spectra at positions within $\sim 2'$ from Sgr A* and the corresponding position-velocity diagrams indicate that the origin of the wide line is related to the CND. The wide line at the position marked '1' (Fig. 6) results due to contributions from different parts of the CND in different velocity ranges (Fig. 8). On the other hand, the declination-velocity diagram corresponding to the position marked '5' (Fig. 9) does not show the features corresponding to the CND as the CND

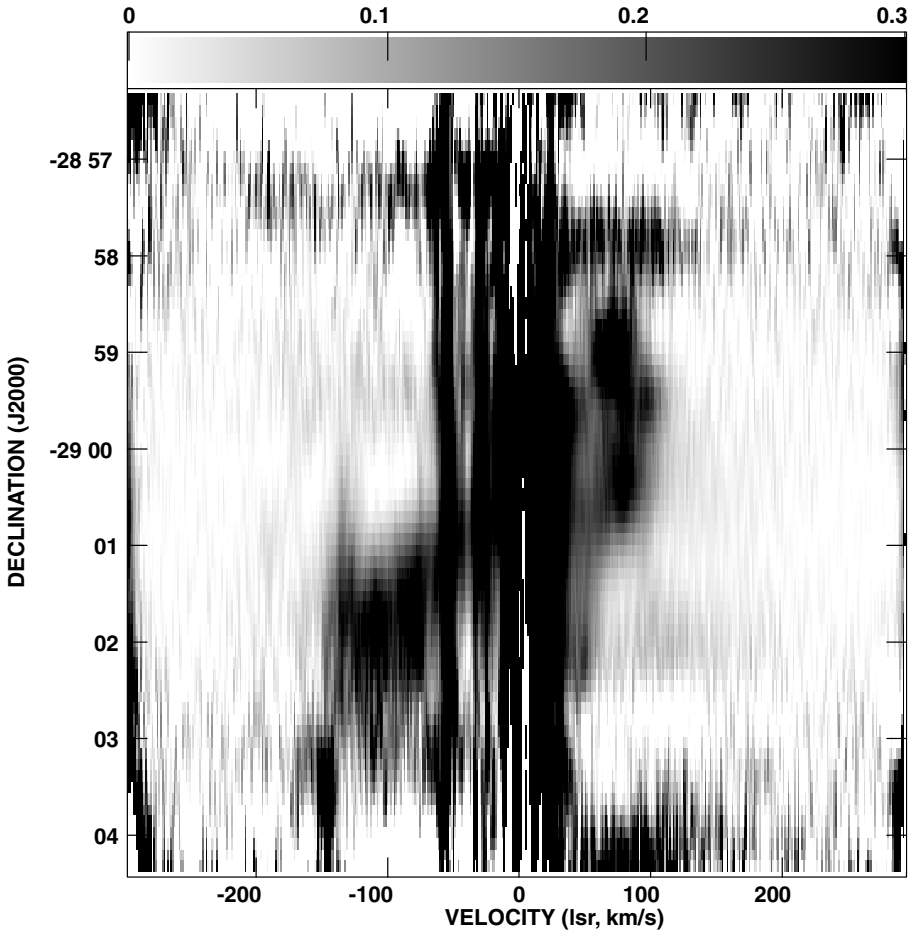

Figure 8. Declination-velocity diagram from the C + D array data at the right ascension of the position marked '1' in Fig. 3. The grey scale is optical depth in the range 0–0.3. The reliable portion of the image is $-29^\circ\ 3' < \delta < -28^\circ\ 57'$. The features to the north of Sgr A* at positive velocities (~ 100 km s^{-1}) and to the south of Sgr A* at negative velocities (~ -100 km s^{-1}) are due to the circumnuclear disk surrounding Sgr A*.

is confined to within $\sim 2'$ of Sgr A*. Consequently, the optical depth spectrum at the position marked '5' (Fig. 7) does not detect a wide line.

The wide line detected in the Parkes Interferometer observations towards Sgr A* was interpreted as a large velocity dispersion line (RS1). The dispersion was attributed to the random motions of a new population of shocked HI clouds in the Galaxy observed along the line of sight towards Sgr A* (RS2). This new population was postulated to be warmer and more abundant (~ 15 clouds/kpc) than the standard cold HI clouds. If such a scenario were correct, a diffuse feature over a range of velocities corresponding to the FWHM of the wide line should have been detected in the declination-velocity diagrams (Figs. 8 and 9). No such feature was detected in these images. The shocked HI cloud picture in this context is thus implausible. Consequently, there are no implications of the wide line to the energetics of the interstellar medium. The current observations

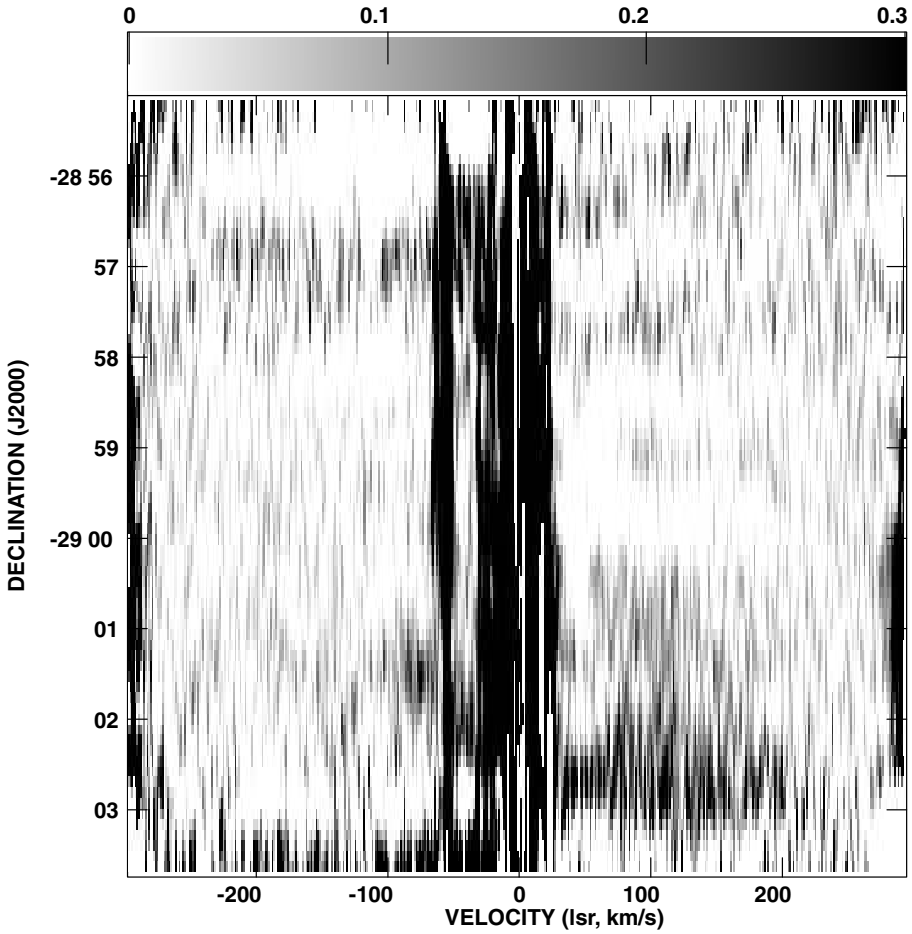

Figure 9. Same as in Fig. 8 but at the right ascension of the position marked '5' in Fig. 3. The CND is not detected in this image since the CND is confined to within $\sim 2^{'}$ from Sgr A*.

have uncovered the origin of the wide HI absorption line towards Sgr A* and have put to rest the related controversies that existed for over two decades.

Acknowledgements

The National Radio Astronomy Observatory (NRAO) is a facility of the National Science Foundation, operated under cooperative agreement by Associated Universities, Inc.

References

Anantharamaiah, K. R., Radhakrishnan, V., Shaver, P. A. 1984, *AA*, **138**, 131.
Bower, G. C., Falcke, H., Herrnstein, R. M., Zhao, J. H., Goss, W. M., Backer, D. C. 2004, *Science*, **304**, 704.
Ekers, R. D., van Gorkom, J. H., Schwarz, U. J., Goss, W. M. 1983, *AA*, **122**, 143.

Gusten, R., Genzel, R., Wright, M. C. H., Jaffe, D. T., Stutzki, J., Harris, A. I. 1987, *ApJ*, **318**, 124.
Kulkarni, S. R., Fich, M. 1985, *ApJ*, **289**, 792.
Liszt, H. S., van der Hulst, J. M., Burton, W. B., Ondrechen, M. P. 1983, *AA*, **126**, 341.
Liszt, H. S., Burton, W. B., van der Hulst, J. M. 1985, *AA*, **142**, 237.
Lo, K. Y., Claussen, M. J. 1983, *Nature*, **306**, 647.
Maeda, Y. *et al*. 2002, *ApJ*, **570**, 671.
Numerical Recipes in FORTRAN 1992, Press, W. H., Teukolsky, S. A., Vetterling, W. T., Flannery, B. P. (Cambridge University).
Pedlar, A., Anantharamaiah, K. R., Ekers, R. D., Goss, W. M., van Gorkom, J. H. *et al*. 1989, *ApJ*, **342**, 769.
Radhakrishnan, V., Goss, W. M., Murray, J. D., Brooks, J. W. 1972, *ApJS*, **24**, 49.
Radhakrishnan, V., Sarma, N. V. G. 1980, *AA*, **85**, 249 (RS1).
Radhakrishnan, V., Srinivasan, G. 1980, *JAA*, **1**, 47 (RS2).
Rekhesh Mohan 2003, PhD Thesis, Jawaharlal Nehru University, New Delhi (RM).
Roberts, D. A., Goss, W. M. 1993, *ApJS*, **86**, 133.
Schwarz, U. J., Ekers, R. D., Goss, W. M. 1982, *AA*, **110**, 100.
Shaver, P. A., Radhakrishnan, V., Anantharamaiah, K. R., Retallack, D. S., Wamsteker, W., Danks, A. C. 1982, *AA*, **106**, 105.